Titanium dioxide nanoparticles induced cytotoxicity, oxidative stress and DNA damage in human amnion epithelial (WISH) cells

Quaiser Saquib [a], Abdulaziz A. Al-Khedhairy [a], Maqsood A. Siddiqui [a], Faisal M. Abou-Tarboush [a], Ameer Azam [c], Javed Musarrat [a,b,*]

[a] Department of Zoology, College of Science, King Saud University, Riyadh, Saudi Arabia
[b] Department of Agricultural Microbiology, Faculty of Agricultural Sciences, Aligarh Muslim University, Aligarh, India
[c] Centre of Nanotechnology, King Abdulaziz University, Jeddah, Saudi Arabia

ARTICLE INFO

ABSTRACT

Titanium dioxide nanoparticles (TiO$_2$-NPs) induced cytotoxicity and DNA damage have been investigated using human amnion epithelial (WISH) cells, as an *in vitro* model for nanotoxicity assessment. Crystalline, polyhedral rutile TiO$_2$-NPs were synthesized and characterized using X-ray diffraction (XRD), UV–Visible spectroscopy, Fourier transform infra red (FTIR) spectroscopy, and transmission electron microscopic (TEM) analyses. The neutral red uptake (NRU) and [3-(4,5-dimethylthiazol-2-yl)-2,5-diphenyltetrazolium bromide] (MTT) assays revealed the concentration dependent cytotoxic effects of TiO$_2$-NPs (30.6 nm) in concentration range of 0.625–10 µg/ml. Cells exposed to TiO$_2$-NPs (10 µg/ml) exhibited significant reduction (46.3% and 34.6%; $p < 0.05$) in catalase activity and glutathione (GSH) level, respectively. Treated cells showed 1.87-fold increase in intracellular reactive oxygen species (ROS) generation and 7.3% ($p < 0.01$) increase in G$_2$/M cell cycle arrest, as compared to the untreated control. TiO$_2$-NPs treated cells also demonstrated the formation of DNA double strand breaks with 14.6-fold ($p < 0.05$) increase in Olive tail moment (OTM) value at 20 µg/ml concentration, vis-à-vis untreated control, under neutral comet assay conditions. Thus, the reduction in cell viability, morphological alterations, compromised antioxidant system, intracellular ROS production, and significant DNA damage in TiO$_2$-NPs exposed cells signify the potential of these NPs to induce cyto- and genotoxicity in cultured WISH cells.

© 2011 Elsevier Ltd. All rights reserved.

1. Introduction

Titanium dioxide (TiO$_2$) is a naturally occurring mineral used in domestic and cosmetic products including anti-fouling paints, coatings, ceramics, additives in pharmaceuticals, food colorants (Jin et al., 2008; Vamanu et al., 2008), and as a sunscreen additive owing to its typical characteristics of surface adsorption, photo-catalysis and UV absorption (Douglas et al., 2000). Titanium either pure or in alloys is also extensively used for a wide range of implanted medical devices, such as dental implants, joint replacements, cardiovascular stents, and spinal fixation devices. However, under mechanical stress or altered physiological conditions such as low pH, titanium-based implants can release large amounts of particle debris (4.47 mg/g dry tissue weight from titanium-alloy (Ti–6Al–4V) implants) both in the micrometer and nanometer size range (Brien et al., 1992; Buly et al., 1992; Arys et al., 1998; Cunningham et al., 2002). It is reported that the biological responses to nanoparticles (NPs) may exceed those elicited by micron-sized particles

(Borm et al., 2006; Nel et al., 2006) due to their small size, high number per given mass, large specific surface area, and generation of free radicals (Lynch et al., 2006). The dimensions of the TiO$_2$-NPs are critical from the toxicity point of view, as the ultrafine TiO$_2$ causes more pronounced toxicity compared with fine TiO$_2$ particles (Driscoll and Maurer, 1991; Oberdörster et al., 1994; Oberdörster, 2000). Ultrafine TiO$_2$ particles ($\leqslant$20 nm) have been shown to induce impairment of macrophage function, persistently high inflammatory reactions, and increased pulmonary retention compared to fine TiO$_2$ (particle size > 200 nm) (Baggs et al., 1997). The TiO$_2$-NPs could be absorbed through inhalation, ingestion and dermal penetration into the body, and distributed in the important organs such as lung (Warheit et al., 2007; Wang et al., 2007), lymph nodes (Bermudez et al., 2004), brain (Thomas et al., 2006), liver and kidney (Wang et al., 2007).

There are growing concerns about the possible influence of NPs on human health, particularly with the exposures during prenatal, pregnancy or early childhood (Lacasana et al., 2005). Nanosized materials including the carboxylic polystyrene, gold and TiO$_2$-NPs are reported to cross the placental tissue (Semmler-Behnke et al., 2007; Tian et al., 2009). In an ex-vivo human placental perfusion model, Wick et al. (2010) demonstrated the uptake of nanosized

---

fluorescently labeled polystyrene beads of 50, 80, 240, and 500 nm across the placental barrier. Also, in animal models, the translocation of TiO$_2$-NPs has been reported in brain of prenatally exposed mice. Since the blood barriers are under developed in the foetus, the NPs could easily pass into brain during the early stages of foetal development. The TiO$_2$-NPs in anatase (crystals of eight-faced tetragonal dipyramids) form, administered subcutaneously to pregnant ICR mice, were found to be transferred to and affected the genital and cranial nerve systems of the offspring (Takeda et al., 2009).

Furthermore, Gurr et al. (2005) demonstrated that anatase-sized (10 and 20 nm) TiO$_2$-NPs in the absence of photoactivation induce oxidative DNA damage, lipid peroxidation, and micronuclei formation, and cause increased hydrogen peroxide and nitric oxide production in human bronchial epithelial (BEAS-2B) cell line. Vevers and Jha (2008) have reported the enhanced level of TiO$_2$-NPs induced DNA damage in presence of UV light in rainbow trout gonadal tissue cells. Whereas, in the goldfish skin cells (GFSk-S1), the TiO$_2$-NPs caused DNA damage in the absence of UV light (Reeves et al., 2008). Also, in human monoblastoid and bronchial epithelial cells, the TiO$_2$-NPs induce apoptosis mainly by destabilizing the lysosomal membrane and lipid peroxidation (Vamanu et al., 2008; Zhao et al., 2009; Hussain et al., 2010). The TiO$_2$ induced DNA damage and apoptosis have also been demonstrated in human lymphocytes, U937 human monoblastoid cells, A549 alveolar epithelial cells, NRK-52E normal rat kidney cells, and A431 human epidermal cells (Vamanu et al., 2008; Gopalan et al., 2009; Park et al., 2007; Barillet et al., 2010; Shukla et al., 2011). However, to the best of our understanding, no systematic study on assessment of the TiO$_2$-NPs cytotoxicity and genotoxicity on cells of placental origin are reported in literature. There are reports that the human amnion epithelial cell line established as WISH (Wistar Institute, Susan Hayflick) cells maintains the similar characteristics of growth, cell morphology, prostaglandin production, and susceptibility to apoptotic agents, as the primary amnion cells (Lundgren et al., 1997; Moore et al., 2002). Perhaps, the stability of these cells makes them more useful for studies that the primary cultures of amnion cells will not tolerate (Kumar et al., 2004). Therefore, the amniotic WISH cells have been chosen as a model in this study, with the aim to assess the effects of sonomechanically synthesized TiO$_2$-NPs on the (i) cell viability as cytotoxic end point, (ii) intracellular ROS production and antioxidative enzymes, (iii) induction of DNA strand breaks, and (iv) progression of normal cell cycle, in order to elucidate the plausible role of TiO$_2$-NPs in evoking toxic responses in WISH cells, as putative markers for placental toxicity.

2. Materials and methods

2.1. Chemicals

Dimethyl sulfoxide (DMSO) cell culture grade, propiodium iodide, Na$_2$-EDTA, Tris [hydroxymethyl] aminomethane, RNAse, 2′,7′-dichlorofluorescin diacetate (DCFH-DA), normal melting agarose (NMA), low melting agarose (LMA), ethyl methanesulphonate (EMS) and neutral red were purchased from Sigma Chemical Company, St. Louis, MO, USA. RPMI-1640, L-glutamine, MTT (3-(4,5-Dimethylthiazol-2-yl)-2,5-diphenyltetrazolium bromide, antibiotic–antimycotic solution, phosphate buffered saline (PBS, Ca^{2+}, Mg^{2+} free) were obtained from Hi-Media Pvt. Ltd. (India). Foetal bovine serum (FBS) was procured from GIBCO-BRL Life Technologies Inc. (Gaithersburg, MD, USA). Culture wares and other plastic consumables used in the study were procured commercially from Nunc, Denmark. Kits for the catalase (Cat # 707002) and glutathione (Cat # 703002) assays were purchased from Cayman Chemicals, USA. Powdered TiO$_2$-NPs (1 mg/ml) were suspended in

Milli-Q water and subjected to sonication using Pro Scientific Inc., USA for 15 min at 40 W to form a homogeneous suspension before the treatments.

2.2. Synthesis and characterization of TiO$_2$-NPs

TiO$_2$-NPs were synthesized using sonomechanical method. In brief, 50 g of bulk TiO$_2$ (rutile form) was taken in 250 ml beaker and 30 ml of methanol was added to form a slurry, which was sonicated for 30 min. The slurry was dried at 100 °C for 12 h in an oven, and the methanol evaporates during drying process. The slurry was then ground in a planetary ball mill, (Retsch, Germany). Initial milling was done for 10 h at 350 rpm and then extended up to 30 h. Finally, the milled slurry was dried at 100 °C for 12 h in an oven. Several techniques were employed for characterizing the finally obtained white powder. The X-ray diffraction (XRD) was used for crystal phase identification and estimation of the average crystallite size. The particle size and morphology of the powder were observed by transmission electron microscope (TEM). UV–visible absorption spectrum was carried out in order to characterize the optical properties of the TiO$_2$-NPs. Fourier transform infra red (FTIR) spectrum was used to study the functional groups and stretching vibrations of the bonds in the TiO$_2$-NP lattice. The NPs aggregation in suspension and secondary particles sizes were estimated using dynamic light scattering (DLS).

2.3. X-ray diffraction analysis

Powdered sample of TiO$_2$-NPs was analyzed using X'pert PRO analytical diffractometer (Rigaku X-ray diffractometer, Japan) using CuKα radiation (λ = 1.54056 Å) in the range of $20° \leqslant 2\theta \leqslant 80°$ at 40 keV. In order to calculate the particle size (D) of TiO$_2$ sample, the Scherrer's relationship ($D = 0.9\lambda/B\cos\theta$) has been used, where, λ is the wavelength of X-ray, B is the broadening of diffraction line measured as half of its maximum intensity in radians and θ is the Bragg's diffraction angle. The particle size of sample has been estimated from the line width of XRD peak.

2.4. UV–visible spectroscopy, FTIR and TEM analyses

The spectra of TiO$_2$-NPs were recorded using a UV–Vis spectrophotometer, Cintra 10e GBC (Victoria, Australia) at wavelengths between 200 and 800 nm. The band gap of TiO$_2$-NPs was determined from the well known Tauc relation, $\alpha h\nu = A(h\nu - Eg)n$ (Tauc et al., 2006), where, $h\nu$ is photon energy, $\alpha = 2.303A/t$ is called the absorption coefficient, A is the absorbance, t is the thickness of the cuvette, E_g is the band gap and n = 2 for indirect band gap semiconductor. The FTIR was employed for examining the functional groups on TiO$_2$-NPs. For FTIR analysis, the dried powder of TiO$_2$-NPs was diluted with spectroscopic grade potassium bromide (KBr) in the ratio of 1:100 and the spectrum was recorded. FTIR measurements were carried out on Perkin–Elmer FTIR spectrophotometer (USA) in the diffuse reflectance mode at a resolution of 4 cm^{-1} in KBr pellets. For TEM analysis, the samples were prepared by dropping the ultrasonically treated TiO$_2$-NPs suspension onto a TEM copper grid and dried at room temperature. A total of six TEM samples were prepared, and at least ten micrographs of each were analyzed to determine the ensemble average of the sample primary particle size. TEM was performed on a Field Emission Transmission Electron Microscope (JEM-2100F, JEOL, Japan) at 200 keV.

2.5. Dynamic light scattering and particle dosimetry

TiO$_2$-NPs stock suspension of 2 mg/ml was prepared in deionized Milli-Q water and sonicated for 15 min at 40 W. Stock suspension was then instantly diluted in the Milli-Q water and RPMI cell

culture medium. Dynamic light scattering was performed on a ZetaSizer-HT, Malvern, UK to determine the hydrodynamic sizes of the TiO_2-NPs in suspensions. The theoretical estimations of exposure, delivered and cellular doses at the nominal media mass concentration of 10 µg/ml of an average secondary TiO_2 particle size of 152 nm in RPMI medium were performed assuming the particles to be spherical, following the simplifying assumptions and Eqs. (1) and (2), as specified by Teeguarden et al. (2007)

$$\text{Surface area concentration} = \frac{\text{mass concentration}}{\text{particle density}} \times \frac{6}{d}$$

$$= \# \text{ Concentration} \times \pi d^2 \qquad (1)$$

$$\# \text{ Concentration} = \frac{\text{mass concentration}}{\text{particle density}} \times \frac{6}{\pi d^3}$$

$$= \frac{\text{Surface area concentration}}{\pi d^2} \qquad (2)$$

where particles are assumed to be spherical, or can be represented as spheres, d is the particle diameter in cm, surface area concentration in cm^2/ml media, mass concentration is in g/ml, # indicates particle number and particle density is in g/cm^3.

2.6. Cell culture and TiO₂-NPs treatment

Human amnion epithelial (WISH) cell line (American Type Culture Collection, accession No. CCL25, Rockville, MD, USA) was maintained in our laboratory and have been used for toxicity analysis of TiO_2-NPs. This cell line was chosen as a model due to its higher stability as compared to the primary cultures of amnion cells (Kumar et al., 2004). Cells were grown in RPMI 1640, supplemented with 10% FBS and antibiotic–antimycotic solution (100×, 1 ml/100 ml of medium) in 5% CO_2 with 95% atmosphere in humidity at 37 °C. Each batch of cells was assessed for cell viability by trypan blue dye exclusion test prior to the experiments and batches showing more than 95% cell viability and passage number between 10 and 15 were used in the study. For TiO_2-NPs treatment, the cells (1×10^4/100 µl/well) in complete RPMI medium were seeded in 96-well plates, and exposed to varying concentrations (0.625–10 µg/ml) of TiO_2-NPs for 24 h at 37 °C. The concentration range and time of exposures were determined based on the NRU and MTT cytotoxicity assays. Similarly related dose ranges have also been used in earlier studies on TiO_2 induced oxidative DNA damage, lipid peroxidation, micronuclei formation, and the hydrogen peroxide and nitric oxide production in human bronchial epithelial (BEAS-2B) cell line and reactive oxygen species production in immortalized brain microglia (BV2) cells (Gurr et al., 2005; Long et al., 2007).

2.7. TiO₂-NPs uptake in WISH cells

The TEM analysis of TiO_2-NPs treated WISH cells for uptake and internalization have been performed following the method, as described by Hussain et al. (2009). Briefly, cells (5×10^4) were seeded in 6 well tissue culture plate and allowed to adhere for 24 h in CO_2 incubator at 37 °C. Cells were then exposed to TiO_2-NPs (10 µg/ml) for 24 h. The untreated and TiO_2-NPs treated cells were harvested and fixed with 10% glutaraldehyde in 0.1 M cacodylate buffer (pH 7.4) for 20 min. Cells were then suspended in 1% OsO_4 in 0.1 M cacodylate buffer (pH 7.4) for 1 h at 4 °C, followed by 1 h incubation in 2% aqueous uranyl acetate at room temperature. The samples were dehydrated in an ethanol series and embedded in low viscosity araldite resin. Ultrafine sections (60 nm thick) were visualized under high vacuum at 100 kV using JEOI-1011 Electron Microscope (JEOL, Tokyo, Japan). The images were captured without any

contrast agent to avoid potential artifacts due the deposition of contrast agent crystals.

2.8. Tetrazolium bromide salt (MTT) assay

The viability of TiO_2-NPs treated WISH cells was assessed by MTT assay, as described by Siddiqui et al. (2010). In brief, cells (1×10^4) were allowed to adhere for 24 h under high humid environment in 5% CO_2-95% atmospheric air at 37 °C in 96-well culture plates. Cells were exposed to TiO_2-NPs in the concentration range of 0.625 to 10 µg/ml for 24 h. Subsequently, MTT (5 mg/ml stock in PBS) was added in the volume of 10 µl/well in 100 µl of cell suspension, and the plate was incubated for 4 h at 37 °C. At the end of incubation period, the aqueous medium was carefully aspirated and 200 µl of DMSO was added to each well and mixed gently. The plate was then kept on a rocker shaker for 10 min at room temperature and the purple color developed was read at 550 nm using microplate reader (Multiskan Ex, Thermo Scientific, Finland). Untreated controls were also run under identical conditions. The probability of TiO_2-NPs interference with the cytotoxicity assay was assessed by measuring the MTT reduction to formazan with ascorbic acid following the method of Belyanskaya et al. (2007). Briefly, the TiO_2-NPs (0.625 to 100 µg/ml) were incubated with 1 mg/ml ascorbic acid in the presence or absence of 1 mg/ml MTT for 60 min at 37 °C. The suspension was centrifuged at 14,000 rpm for 30 min and the supernatant was discarded. The precipitate containing the purple formazan product was dissolved in 1 ml of 90% ethanol and sonicated in an ultrasonic bath (Ultrasonic Cleaners, Jeiotech, UC-10, Seoul, Korea) at 25 °C for 5 min. The suspension was again centrifuged at 3000 rpm for 5 min, and the absorbance of the dissolved formazan was measured at 550 nm using UV–visible spectrophotometer (Evolution 300 LC, Thermo Scientific, USA).

2.9. Neutral red uptake (NRU) assay

NRU assay was carried out following the protocol described by Siddiqui et al. (2008). Briefly, cells were exposed to TiO_2-NPs in the concentration range of 0.625 to 10 µg/ml for 24 h. After the exposure time, medium was aspirated and cells were washed twice with PBS, and incubated for 3 h in a medium supplemented with neutral red (50 µg/ml). Medium was washed off rapidly with a solution containing 0.5% formaldehyde and 1% calcium chloride. Cells were subjected to further incubation of 20 min at 37 °C in a mixture of acetic acid (1%) and ethanol (50%) to extract the dye and the absorbance was read at 540 nm on microplate reader. The values were compared with control set run under identical conditions. The probability of TiO_2-NPs interference with the assay was tested by measuring the reactivity of NR dye with TiO_2-NPs in the absence of cultured cells. Briefly, the TiO_2-NPs in the concentration range of 0.625 to 20 µg/ml were mixed with NR dye (50 µg/ml) in complete RPMI medium, in a total reaction volume of 100 µl in a microtitre plate. The mixture was incubated at 37 °C for 3 h. The absorbance was read at 540 nm using a microplate reader (Multiskan Ex, Thermo Scientific, Finland).

2.10. Effect of TiO₂-NPs on catalase activity

Catalase activity of the cells treated for 24 h with varying concentrations (0.625 to 10 µg/ml) of TiO_2-NPs was measured using commercially available kit (Cayman Chemicals, USA). In brief, the TiO_2-NPs exposed cells were sonicated in cold buffer (50 mM potassium phosphate, pH 7.0, containing 1 mM EDTA) and centrifuged at 10,000 rpm for 15 min at 4 °C. The supernatant (20 µl) was collected followed by the addition of 100 µl of assay buffer and 30 µl of methanol in each well of the 96-well plate. Reaction

was initiated by adding 20 μl of hydrogen peroxide as a substrate and incubated on shaker for 20 min at room temperature. The reaction was stopped by adding 30 μl of potassium hydroxide. To this mixture, 30 μl of 4-amino-3-hydrazino-5-mercapto-1,2,4-triazole (purpald) was added as chromogen, and incubated for 10 min followed by the addition of 10 μl potassium periodate. The purple color formaldehyde product formed was measured colorimetrically at 540 nm using a microplate reader.

2.11. Effect of TiO₂-NPs on glutathione (GSH) level

The changes in GSH level in TiO₂-NPs exposed cells were determined using a commercially available kit (Cayman Chemicals, USA). In brief, TiO₂-NPs (0.625 to 10 μg/ml) treated cells for 24 h were homogenized in cold MES buffer (50 mM, pH 6.0, containing 1 mM EDTA). The homogenate was centrifuged at 10,000 rpm for 15 min at 4 °C, and the supernatant was collected and deproteinated. The samples (50 μl) were transferred to respective wells in 96-well plate, and 150 μl freshly prepared reagents and enzyme mixtures were added and the absorbance was read after 25 min at 405 nm using a microplate reader.

2.12. Reactive oxygen species (ROS) measurement

Intracellular ROS production was determined in WISH cells using a fluorescent probe DCFH-DA following the method of Wu et al. (2007). Cells were treated with increasing concentrations of TiO₂-NPs (0.625 to 10 μg/ml) for 24 h and harvested by spinning at 3000 rpm for 5 min. The pellet was washed twice with cold PBS and resuspended in 500 μl of PBS. Cells were then incubated with DCFH-DA (5 μM) for 60 min at 37 °C in dark. Immediately after incubation, the cells were washed twice with PBS and finally suspended with 500 μl PBS. DCFH-DA stained cells without TiO₂-NPs treatment and H₂O₂ (100 μM) were taken as negative and positive controls, respectively. The fluorescence was recorded upon excitation at 488 nm. Green fluorescence from 2′,7′-dichlorofluorescein (DCF) was measured in the FL1 Log channel through 525 nm band-pass filter on Beckman Coulter flow cytometer (Coulter Epics XL/Xl-MCL, USA). The interference of TiO₂-NPs with fluorescent DCF was also assessed under acellular conditions following the method of Messer et al. (2006). In brief, 500 μl of DCFH-DA stock (500 μM) was mixed with equal volume of 10 mM NaOH. The mixture was incubated at room temperature for 30 min in dark for the hydrolysis of diacetate ester. Prior to incubation with the TiO₂-NPs, the solution was neutralized by phosphate buffer (pH 7.4). Subsequently, the TiO₂-NPs in increasing concentrations (0.625 to 20 μg/ml) were mixed with 5 and 10 μM DCFH in a final reaction volume of 100 μl in a 96 well microtitre plate. The plate was incubated at 37 °C for 60 min. The fluorescence of DCF was measured at 485 nm excitation and 520 nm emission wavelengths using microplate fluorometer (Thermo Scientific Fluoroskan Ascent, Finland).

2.13. Assessment of cell cycle progression of TiO₂-NPs treated cells

WISH cells treated with increasing concentrations (0.625 to 10 μg/ml) of TiO₂-NPs for 24 h were harvested and centrifuged at 3000 rpm for 5 min, and the pellet was resuspended in 500 μl of PBS. Cells were fixed with equal volume of chilled 70% ice-cold ethanol, and incubated at 4 °C for 1 h. After two successive washes, the cell pellet was again suspended in PBS and stained with propidium iodide (50 μg/ml) solution containing 0.1% Triton X-100 and 0.5 mg/ml RNAase A for 1 h at 37 °C in dark. The red fluorescence of 10,000 events of propidium iodide stained cells were acquired in FL4 Log channel through a 675 nm band-pass filter using flow cytometer (Darzynkiewicz et al., 1992). The data were analyzed

excluding the cell debris, characterized by a low FSC/SSC, using Beckman Coulter flow cytometer (Coulter Epics XL/Xl-MCL, USA and System II Software, Version 3.0.

2.14. Assessment of DNA damage by neutral comet assay

TiO₂-NPs induced strand breaks in DNA were assessed by neutral comet assay, as described by Omidkhoda et al. (2007). Slide preparation was done following the method of Saquib et al. (2009). In brief, the cells at a density of 6.0×10^4 cells/well were exposed to varying concentrations of TiO₂-NPs (0.625 to 20 μg/ml) in a 12 well plate for 6 h at 37 °C. The cells were washed with serum free medium and harvested by adding 0.065% trypsin and incubated at 37 °C. The cell suspension was centrifuged at 3000 rpm, 5 min and the pellet was resuspended in 100 μl of PBS. The cells were mixed with 100 μl of 1% LMA and layered on one-third frosted slides, pre-coated with NMA (1% in PBS) and kept at 4 °C for 10 min. After gelling, another layer of 90 μl of LMA (0.5% in PBS) was added. The cells were lysed in a lysing solution for overnight. After washing with TBE buffer, the slides were subjected to neutral electrophoresis in cold TBE (Tris-base, 90 mM; boric acid, 90 mM; Na₂EDTA, 2.5 mM) buffer. Electrophoresis was performed at 1 V/cm for 30 min (16 mA, 32 V) at 4 °C. All preparative steps were conducted in dark to prevent secondary DNA damage. Each slide was stained with 75 μl of 20 μg/ml ethidium bromide solution for 5 min. The slides were analyzed at 40× magnification (excitation wavelength of 515–560 nm and emission wavelength of 590 nm) using fluorescence microscope (Nikon ECLIPSE E600, Japan) coupled with charge coupled device (CCD) camera. Images from 50 cells (25 from each replicate slide) were randomly selected and subjected to image analysis using software Comet Assay IV (Perceptive Instruments, Suffolk, UK).

2.15. Statistical analysis

Data were expressed as mean ± S.D for the values obtained from at least three independent experiments. Statistical analysis was performed by one-way analysis of variance (ANOVA) using Dunnett's multiple comparisons test (Sigma Plot 11.0, USA). The level of statistical significance chosen was $^*p < 0.05$, unless otherwise stated.

3. Results

3.1. XRD and TEM analysis of TiO₂-NPs

The X-ray diffraction pattern of TiO₂-NPs obtained by sonomechanical method is shown in Fig. 1. The peaks were indexed using Powder × software and were found corresponding with the tetragonal rutile structure of TiO₂ (ICDD card No. 78–2485). No impurity phase was observed in the sample. The average crystallite size of the samples was calculated using Debye Scherrer's formula. The estimated size corresponding to the most intense crystallographic plane (110) was determined to be 30.6 nm. The typical TEM image shown in Fig. 1 (inset) clearly suggests that most of the TiO₂-NPs are crystallites with polyhedral morphologies.

3.2. UV- Vis absorption characteristics of TiO₂-NPs

Fig. 2A shows the optical absorbance spectra of TiO₂-NPs. The absorbance is expected to depend on several factors, such as band gap, oxygen deficiency and impurity centers. The absorbance spectrum exhibits an absorption edge around 280–320 nm, which may be due to the photo-excitation of electrons from valence band to conduction band. The Tauc plot between $(\alpha h\nu)^{1/2}$ and $h\nu$
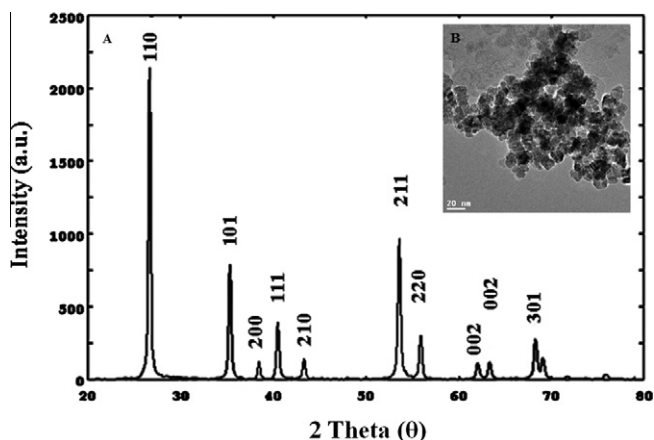
Fig. 1. (A) X-ray powder diffraction (XRD) analysis for phase identification of sonomechanically synthesized crystalline TiO$_2$-NPs. (B) Inset shows the TEM image of TiO$_2$-NPs at 200 keV.
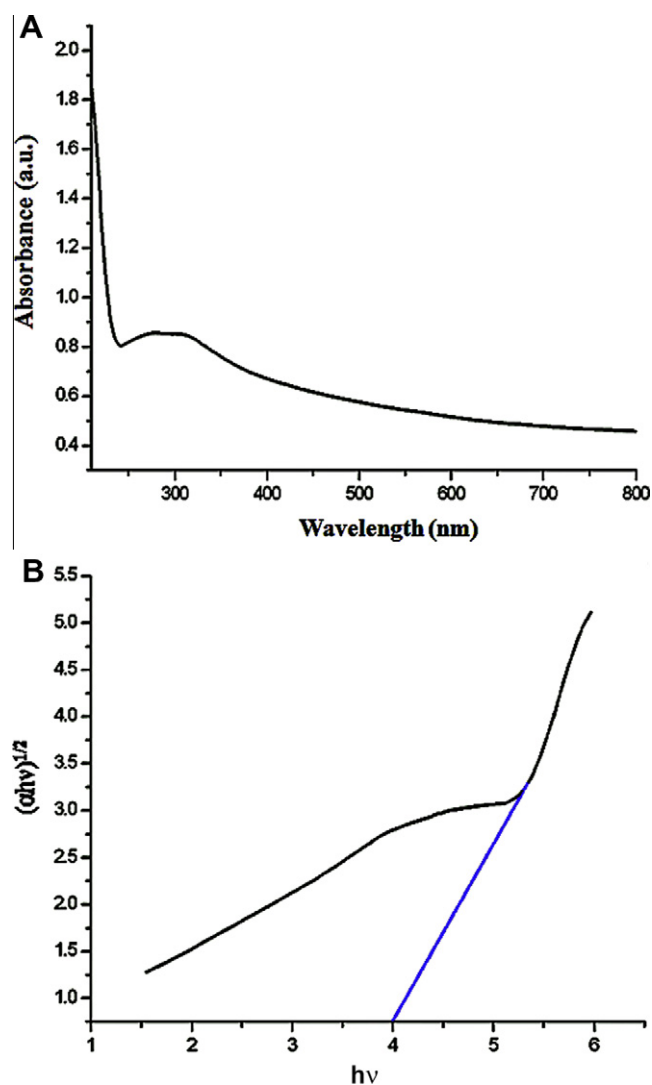

Fig. 2. Absorption characteristics of TiO$_2$-NPs. Panel (A) shows the absorption spectrum of TiO$_2$-NPs; whereas, the panel (B) depicts the Tauc plot for determining optical gap in amorphous material. The axes represent the quantity $h\nu$ (the energy of light) on the abscissa and the quality $(\alpha h\nu)^{1/2}$ on the ordinate, where α is the absorption coefficient of the material, as a function of TiO$_2$-NPs.
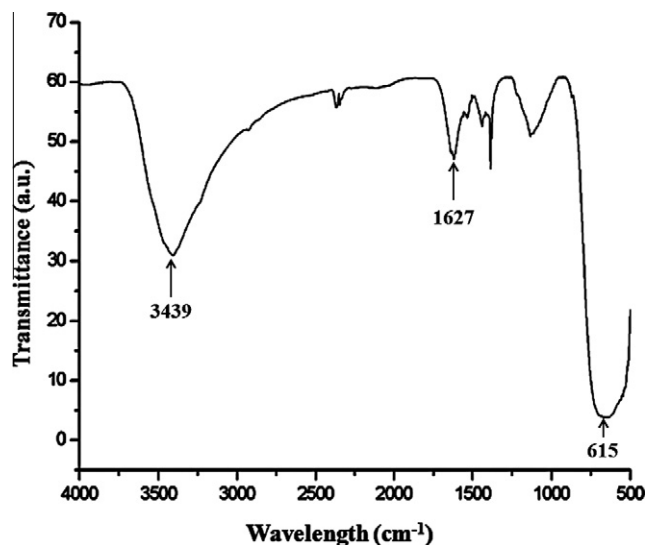

Fig. 3. FTIR spectrum of TiO$_2$-NPs. The peak located at 615 cm^{-1} represents the characteristic vibration of Ti–O bond in the TiO$_2$ lattice. The band at 1627 cm^{-1} signifies the molecular water bending mode, while the broad peak at 3439 cm^{-1} corresponds to –OH stretching vibration in the sample.

of TiO$_2$-NPs (rutile) is shown in Fig. 2B. The extrapolation of the linear region of a plot of $(\alpha h\nu)^{1/2}$ vs $h\nu$ provided the value of the optical band gap E_g. The band gap measured from Tauc plot was determined to be 4.0 eV, which is higher than the value of E_g for bulk TiO$_2$ (3.2 eV). This increase in the value of band gap confirms the reduction of the particle size. Moreover, the higher value of band gap indicates the higher photooxidation as well as photoreduction ability of TiO$_2$-NPs.

3.3. FTIR analysis of TiO$_2$-NPs

The FTIR spectrum shown in Fig. 3 was recorded in solid phase using KBr pellets technique in the region of 4000–500 cm^{-1} with the resolution of 4 cm^{-1}. The peak located at 615 cm^{-1} is the characteristic vibration of the Ti–O bond in the TiO$_2$ lattice. The band at 1627 cm^{-1} is assigned to the molecular water bending mode, while the broad peak at 3439 cm^{-1} shows the presence of –OH stretching vibration. The broad peak appearing at 3439 cm^{-1} was assigned to fundamental stretching vibration of O-H hydroxyl group, which was further confirmed by a weak band at about 1627 cm^{-1} caused by bending vibration of coordinated H$_2$O. The band observed at 650 cm^{-1} is assigned to the Ti-O stretching vibration in the TiO$_2$ lattice. The above assignments are in good agreement with the results reported in literature (Yoko et al., 1990; Zhang and Gao, 2002; Zhang et al., 2002; Gao et al., 2004).

3.4. Hydrodynamic diameter of TiO$_2$-NPs in culture medium

The results of hydrodynamic size of the TiO$_2$-NPs using dynamic light scattering are shown in Fig. 4. The dispersion of TiO$_2$-NPs of average size 30.6 nm was heterogeneous due to the presence of both the primary particles and larger aggregates. The distribution curves show the TiO$_2$-NPs with a small population of an average 13 nm particle size and larger aggregates of 152 nm in RPMI medium as compared to the much larger particle aggregates of 380 nm in deionized Milli-Q water.

3.5. TEM analysis for TiO$_2$ uptake and accumulation in WISH cells

TEM of WISH cells exposed to TiO$_2$-NPs for 24 h exhibit the aggregates of NPs, localized either inside the vesicles, as shown
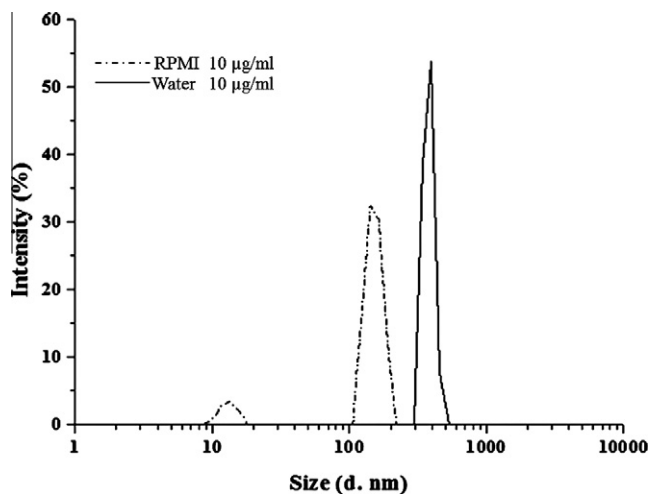
Fig. 4. Size distribution and secondary size analysis of TiO$_2$-NPs in suspension. Dynamic light scattering (DLS) analysis of TiO$_2$-NPs (10 µg/ml) after suspending in RPMI culture medium and Milli-Q water to determine the size distributions and hydrodynamic diameters of NPs.

3.6. TiO$_2$-NPs induced cytotoxicity in WISH cells

Cells exposed to TiO$_2$-NPs for 24 h exhibited a concentration dependent decline in the cell survival as compared to untreated control in MTT assay. The data exhibited about 9.6%, 17.5%, 20.0%, 24.3% and 24.5% reduction in cell viability at varying particle mass concentrations of 0.625, 1.25, 2.5, 5.0 and 10 µg/ml, respectively vis-à-vis untreated control (Fig. 6). Furthermore, the results related to the influence of TiO$_2$-NPs on ascorbic acid induced MTT reduction under acellular conditions, showed no interference in the development of purple colored MTT-formazan product formation up to 40 µg/ml. However, addition of TiO$_2$-NPs at higher concentrations of 80 µg/ml and above, resulted in significant ($p < 0.010$) increase in the color intensity, as compared to the control (Supplementary Fig. S1).

The results of neutral red (3-amino-7-dimethyl-amino-2-methylphenazine hydrochloride) uptake (NRU) are also shown in Fig. 6. The data exhibited a concentration dependent decline in the survival of cells exposed to TiO$_2$-NPs for 24 h. The cellular uptake of neutral red is proportional to the number of viable cells. A significant TiO$_2$-NPs cytotoxicity has been noticed at concentrations above 1.25 µg/ml. The percent decline in the cell viability at concentrations of 2.5, 5 and 10 µg/ml was determined to be 13.1%, 19.7% and 42.5%, respectively as compared to the untreated control. Under acellular conditions, the TiO$_2$-NPs did not show any interference with NR dye in concentration range of 0.625 to 10 µg/ml, However, some interference occurred at a higher concentration of 20 µg/ml, marked with a significant increase ($p < 0.05$) in the absorbance at 540 nm, as compared to the control (Supplementary Fig. S2).

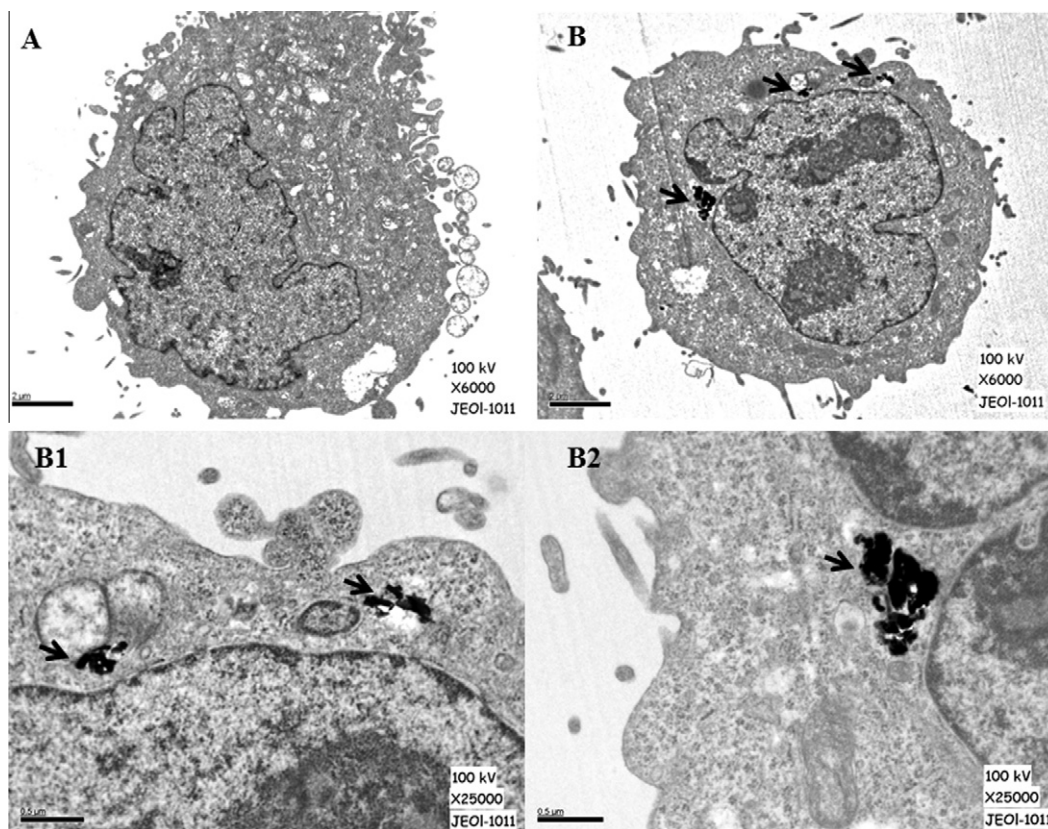in the representative Fig. 5 B, B1 or free in the cytoplasm (Fig. 5 B2). More than 85% of the analyzed cell sections exhibited internalized TiO$_2$-NPs aggregates. Comparison with the untreated controls confirmed the presence of aggregated NPs and nuclear condensation in treated cells.

Fig. 5. TEM analysis of internalized TiO$_2$-NPs in WISH cells. Cells after 24 h exposure to RPMI medium alone (control) and TiO$_2$-NPs (10 µg/ml) in RPMI medium were analyzed by TEM. The representative images in the panels are depicted as (A) control, ×6000; (B) TiO$_2$-NPs treated, ×6000; (B1 and B2) TiO$_2$-NPs treated cells, same as in panel B at higher magnifications of ×25,000. Dark arrows indicate the accumulated TiO$_2$-NPs in vesicles and cytoplasm. Peripheral chromatin condensation is apparent in panel B as compared to control (panel A).
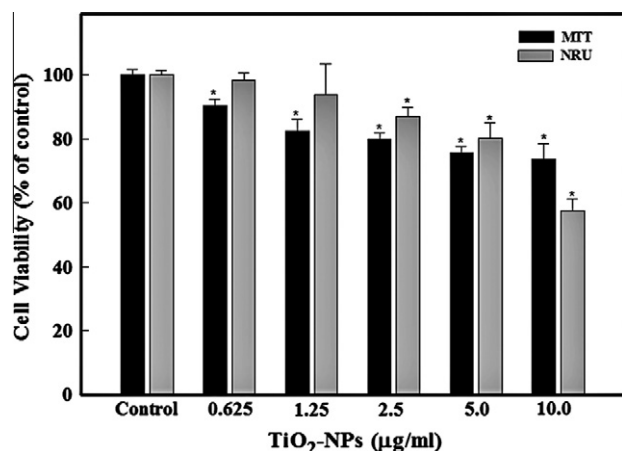
Fig. 6. Cytotoxicity assessment of TiO_2-NPs in WISH cells exposed for 24 h. Histogram shows the percent cell viability using MTT and NRU assays, respectively. Data are the mean ± SD of three independent experiments. $^*p < 0.05$ vs control.
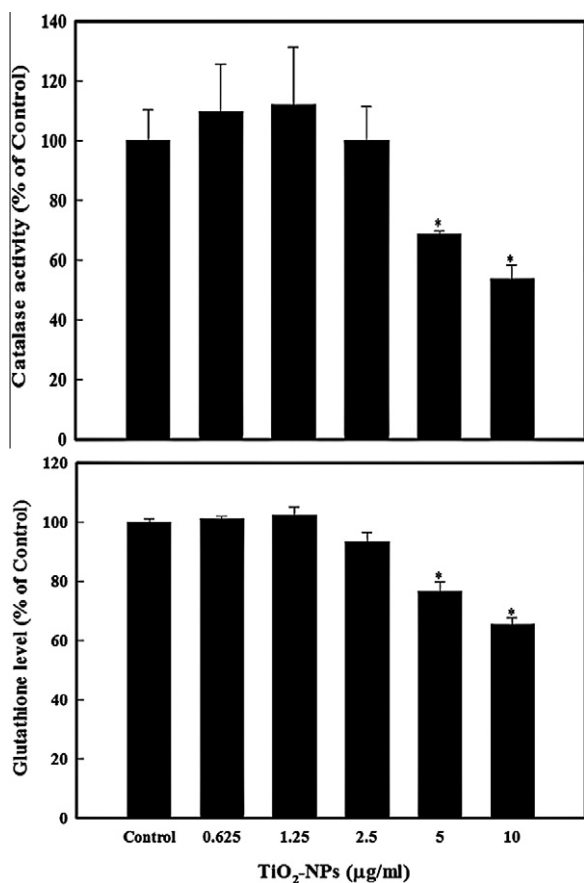

Fig. 8. Flow cytometric analysis of intracellular ROS generation in WISH cells treated with TiO_2-NPs exposed for 24 h. Panel A shows the representative spectra of fluorescent DCF as a function of TiO_2-NPs concentration. Panel B exhibits the comparative analysis of the fluorescence enhancement of DCF with increasing TiO_2-NPs concentrations. CtI and CtII represent the negative and positive (H_2O_2, 100 μM) controls, respectively. Each histogram represent the values of mean ± SD of three independent experiments. $^*p < 0.05$, $^{**}p < 0.01$ vs control.

Fig. 7. Effect of TiO_2-NPs on antioxidative enzymes, catalase and glutathione (GSH) levels in WISH cells exposed for 24 h. Each histogram represents the mean ± SD of three independent experiments. $^*p < 0.05$ vs control.

3.7. TiO_2-NPs mediated change in catalase and glutathione (GSH) levels

Catalase and GSH levels of TiO_2-NPs treated cells were measured to assess the extent of oxidative stress in WISH cells. Fig. 7 shows a significant decrease in the catalase activity in WISH cells treated at higher TiO_2-NPs concentrations vis-à-vis untreated control cells. Considering the enzyme activity in untreated control as
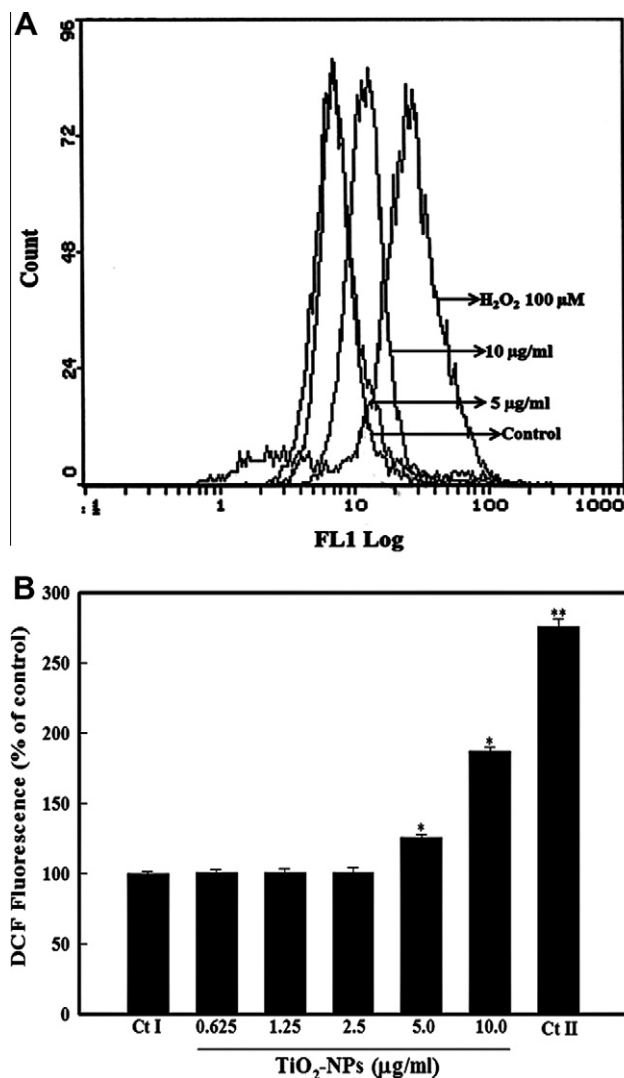
100%, the reductions in catalase activity were determined to be 31.4% and 46.3% ($p < 0.05$) at 5 and 10 μg/ml, respectively. Further, the cells exposed to TiO_2-NPs for 24 h have also exhibited depletion of GSH level at higher concentrations (Fig. 7). Compared to the untreated control, the percent decline in the glutathione levels at 5 and 10 μg/ml were determined to be 23.3 and 34.6% ($p < 0.05$), respectively.

3.8. TiO_2-NPs-induced intracellular ROS generation

The TiO_2-NPs induced intracellular ROS generation in WISH cells was analyzed by flow cytometry using a fluorescence probe DCFH-DA. Fig. 8A shows a significant shift in the DCF fluorescence peak, exhibiting increased ROS production at 5.0 and 10 μg/ml concentrations of TiO_2-NPs in treated cells. Almost 1.2- and 1.87-fold enhancements in the levels of intracellular ROS were determined after 24 h of TiO_2-NPs exposure at 5 and 10 μg/ml concentrations, respectively as compared with the untreated control cells (Fig. 8B). However, no significant changes in the fluorescence intensity was
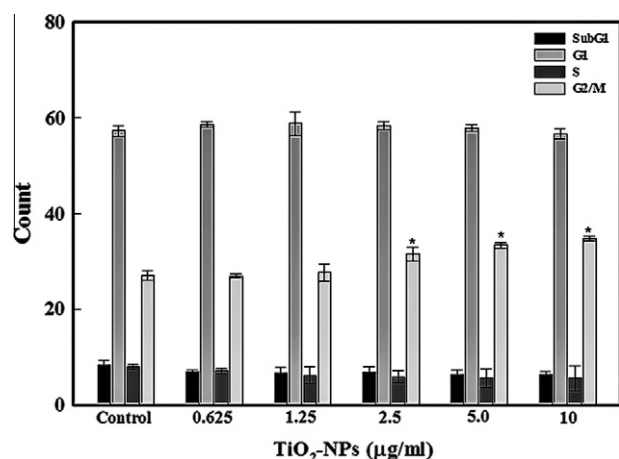
Fig. 9. Effect of TiO$_2$-NPs on cell cycle progression in WISH cells treated for 24 h. Each histogram represents mean ± SEM values of different phases of cell cycle obtained from three independent experiments done in triplicate tubes. *$p < 0.01$ as compared to control. G$_1$, S, G$_2$/M represents the percentage of cells present in normal phases of cell cycle, SubG$_1$ represents percentage of cells undergone apoptosis/necrosis.

observed after interaction of TiO$_2$-NPs up to 20 µg/ml with 5 and 10 µM DCFH under acellular conditions (Supplementary Fig. S3). Also, the lower concentrations (0.625 to 2.5 µg/ml) of TiO$_2$-NPs did not show any significant change in the intracellular ROS levels. Therefore, the spectra at low concentrations overlaps with the control and are not shown in Fig. 8A.

3.9. Effect of TiO$_2$-NPs on cell cycle progression

The results shown in Fig. 9 exhibit the effect of TiO$_2$-NPs on cell cycle progression, as measured in terms of DNA content of the total cell population. After 24 h of TiO$_2$-NPs exposure, the treated cells at

1.25 µg/ml and higher concentrations showed a significant G$_2$/M cell cycle arrest. The mean ± SEM values of three independent experiments exhibited change in DNA contents to the extent of 31.7 ± 1.04, 33.1 ± 0.57, and 34.4 ± 0.76% ($p < 0.01$) at G$_2$/M phase at 2.5, 5.0, and 10 µg/ml concentrations, respectively, as compared to 27.1 ± 0.31% in untreated control cells.

3.10. TiO$_2$-NPs-induced DNA damage

Cells exposed to varying concentrations of TiO$_2$-NPs for 6 h have exhibited a significant induction ($p < 0.05$) in DNA damage at a concentration of 20 µg/ml. The representative images of DNA damage obtained with the neutral comet assay of TiO$_2$-NPs treated WISH cells are shown in Fig. 10A. Treated cells at this concentration exhibited 14.6-fold increase in Olive tail moment (OTM) value as compared to the untreated control (Table 1). The data generated in term of OTM reveals the product of tail length and the fraction of total DNA in the tail. It incorporates a measure of both the smallest detectable size of migrating DNA (reflected in the comet tail length) and the number of relaxed/broken pieces (represented by the intensity of DNA in the tail). The frequency distribution analysis of treated cells at the highest concentration of 20 µg/ml exhibited the extent of DNA damage comparable to positive control (EMS, 1 mM) (Fig. 10B).

4. Discussion

The synthesis and applications of metal oxide NPs are consistently expanding due to their distinctive physico-chemical characteristics, and increased industrial and medical applications. This has evoked serious concerns about their potential impact on the environment and human health. Owing to their small aerodynamic diameter, the ultrafine particles (<100 nm) from natural and anthropogenic sources including viruses, biogenic magnetite, ferritin, metal oxides, fullerenes, carbon, polymers and other fumes
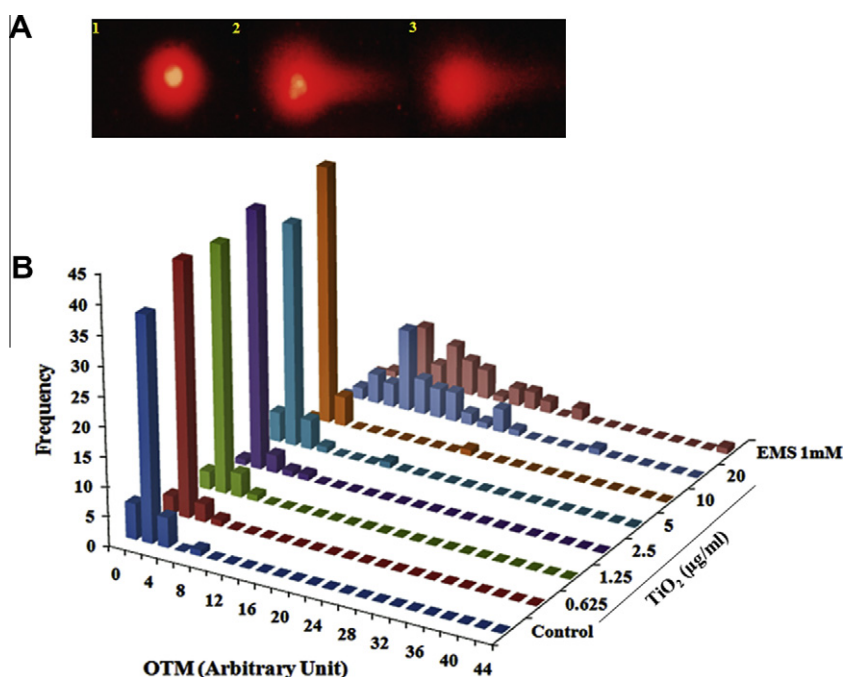

Fig. 10. TiO$_2$-NPs induced strand breaks in cellular DNA of WISH cells. Panel (A) shows the representative epi-fluorescence images of DNA damage in neutral comet assay, as (1) untreated control; (2) EMS (1 mM) as positive control; (3) TiO$_2$-NPs (20 µg/ml). Panel (B) shows the percent distribution of DNA damage in WISH cells treated with varying concentrations of TiO$_2$-NPs for 6 h. Olive tail moment (OTM) values were determined following the algorithm (Olive Tail Moment = (Tail Mean – Head Mean) × Tail % DNA/100) using Comet Assay IV software.

Table 1
TiO$_2$-NPs induced DNA damage in WISH cells, analyzed using different parameters of comet assay.

Groups	Olive tail moment (arbitrary unit)	Tail length (µm)	Tail intensity (%)
Control	0.66 ± 0.013	40.46 ± 0.19	4.21 ± 0.29
EMS (1 mM)	11.08 ± 0.10*	107.50 ± 0.29*	26.70 ± 0.19*
TiO$_2$-NPs (µg/ml)			
0.625	0.62 ± 0.02	42.13 ± 0.10	3.43 ± 0.22
1.25	0.86 ± 0.05	40.85 ± 0.22	5.33 ± 0.29*
2.5	0.81 ± 0.19	40.35 ± 0.20	4.71 ± 0.11
5.0	0.90 ± 0.08	42.57 ± 0.10	4.21 ± 0.63
10	1.15 ± 0.71	41.86 ± 0.19	5.62 ± 0.43*
20	9.66 ± 0.12*	106.61 ± 0.29*	23.94 ± 0.66*

Data represent the mean ± SD of three independent experiments done in duplicate.
*$p < 0.05$; EMS: Ethyl methanesulphonate.

may contaminate ambient air, penetrate deep into the lungs, and reach different body organs through the blood circulatory system (Oberdörster et al., 2005). The tendency of TiO$_2$-NPs to readily diffuse through the protective cellular barriers may also involve risks to human health, and warrants systematic and in-depth investigation of their possible toxicological effects. Therefore, in this study, we have determined the cytotoxicity and genotoxicity of crystalline TiO$_2$-NPs using human amniotic (WISH) cells for understanding the trans-placental toxicity under *in vitro* conditions. WISH cells have been used as a model in earlier studies to assess the oxidative stress and its impact on gestational prostanoid metabolism and apoptosis in fetal membrane (Keelan et al., 2001; Biondi et al., 2002; Kumar et al., 2004). The sonomechanically synthesized and well characterized polyhedral rutile TiO$_2$-NPs, suspended in RPMI medium were used for cellular treatment and toxicity assessment in cultured WISH cells. Since, the primary and secondary sizes of the NPs are regarded as important parameters for *in vitro* cytotoxicity in a cell culture medium, therefore, the behavior of TiO$_2$-NPs in cell culture medium was evaluated through dynamic light scattering (DLS), to understand the extent of aggregation and secondary size of these NPs before cellular exposure. DLS is widely used to determine the size of brownian NPs in colloidal suspensions in the nano and submicron ranges (Berne and Pecora, 2000). The average hydrodynamic particles diameters (secondary TiO$_2$-NPs particle sizes) in RPMI medium were determined to be much smaller (152 nm) as compared to Milli-Q water (380 nm), which indicates relatively lesser particle aggregation in medium as compared to water. The presence of variable sized (13 to 152 nm) TiO$_2$-NPs aggregates in cell culture medium corroborates well with the earlier reports (Singh et al., 2007; Xia et al., 2006; Limbach et al., 2005). Thus, the DLS data revealed the formation of TiO$_2$-NPs aggregates in the RPMI cell culture medium, which were also found to be internalized in the TEM images of the treated cells. These aggregated NPs in culture medium, have been reported to enter into cells mainly through endocytosis, and their localization in the vacuoles and cell cytoplasm of the exposed cells corresponds well with the observations of Hussain et al. (2009, 2010).

Assessment of TiO$_2$-NPs cytotoxicity through the MTT and NRU assays exhibited the dose dependent toxic effects on cell viability in a concentration range of 0.625 to 10 µg/ml. In context of dose, it is important to realize the significance of nominal and effective dosimetry of NPs in cytotoxicity assays. Teeguarden et al. (2007) suggested that owing to their small size and large surface area, the insoluble NPs are not affected by the gravitational force and generally form stable suspensions or sols. Such NPs might cause problems in the *in vitro* assay systems, as the cells adhering to the bottom of a culture plate may not be exposed to the majority of nanoparticles in suspension. Based on the equations (1) and

(2), specified in the methodology section, the TiO$_2$-NPs (10 µg/ml) treatment to WISH cells, adhered as monolayer at the bottom of the 96 well plates (surface area of 0.36 cm^2) was theoretically estimated to be equivalent to the exposure dose of 1.27×10^8 particles/ml, delivered dose of 3.52×10^8 particles/cm^2 and cellular dose of 1.56×10^4 particles/cell in RPMI medium. Significant cytotoxicity, intracellular ROS generation, and to some extent G$_2$/M cell cycle arrest were induced at the above specified treatment dose, and attributed to TiO$_2$-NPs mediated oxidative stress in the WISH cells. Thus, the results suggest that the TiO$_2$-NPs in the form of a heterogeneous suspension of primary (30.6 nm) and secondary (152 nm) sizes are accessible to the cells in RPMI medium and exhibited the toxic effects. It is likely due to the convection forces in sols, as also suggested by Lison et al. (2008), that these particles may reach to the target cells and exert their potential toxicity.

The morphological analysis of TiO$_2$-NPs treated cells explicitly demonstrated the toxicity, manifested as detachment of the adherent cells at increasing concentrations of TiO$_2$-NPs (results not shown). These results are in agreement with the cellular detachment and morphological changes observed in fish cell line (RTG-2 cells) by Vevers and Jha (2008). The cytotoxic effect at the higher concentration of 10 µg/ml was more pronounced with the NRU vis-à-vis MTT assay, which could be attributed to a greater lysosomal damage as compared to the mitochondria. The results also support the observations of Hussain et al. (2010), who have showed that the TiO$_2$-NPs do not cause any significant loss of mitochondrial potential, whereas, the lysosomal membrane destabilization occurs, which further leads to the release of lysosomal proteases like cathepsin B, and may directly cause proteolysis or activate caspases, as a pathway for TiO$_2$-NP induced death in bronchial epithelial (16HBE14o-) cells.

Biochemical analysis of the cell extracts, flow cytometry and comet data revealed the TiO$_2$-NPs induced changes in the levels of oxidative markers (GSH and catalase), intracellular ROS generation and consequent DNA damage. The data revealed significant depletion in GSH level and catalase activity in TiO$_2$-NPs treated cells at 5 and 10 µg/ml, as compared to the untreated control. The results support the study of Nemmar et al. (2011) on the rutile Fe-doped TiO$_2$ nanorods induced dose dependent decrease in the SOD and GSH levels in the hepatic and heart tissues of rats. The results also corroborate the earlier reports on TiO$_2$-NPs induced ROS production in bronchial epithelial cell line (BEAS-2B) at 10 µg/ml concentration (Gurr et al., 2005). However, Hussain et al. (2009) reported ROS production in bronchial epithelial cell line (16HBE14o-) at 50 and 100 µg/ml. Also, significant intracellular ROS production has been demonstrated in the human epidermal (A431) and brain microglia (mouse BV2) cells at TiO$_2$-NPs doses of 80 µg/ml and 25 µg/ml, respectively (Long et al., 2007; Shukla et al., 2011). Thus, the dose comparison of our study with earlier reports suggests the induction of oxidative stress in WISH cells at relatively lesser concentrations of TiO$_2$-NPs.

Surface reactivity has been suggested to plays an important role in ROS production by NPs (Stone et al., 1998; Oberdörster et al., 2005). Significant ROS generation at 5.0 µg/ml ($p < 0.05$) and 10 µg/ml ($p < 0.01$) concentrations of TiO$_2$-NPs signifies that the primary mechanism of NPs induced toxicity is due to oxidative stress, resulting in damage to cellular membranes and biological macromolecules, as reported earlier (Dalton et al., 2002; Donaldson and Stone, 2003; Nel et al., 2006; Shukla et al., 2011). Our results have also demonstrated that the TiO$_2$-NPs induces DNA damage at a critical concentration of 20 µg/ml. The data suggest that the TiO$_2$-NPs at lower concentrations up to 10 µg/ml modulates the antioxidant enzymes levels, whereas, at higher concentrations, the cellular DNA repair machinery may be adversely affected. Consequently, the unrepaired DNA damage was detected upon single cell gel electrophoresis under neutral assay conditions, which

substantiates the earlier studies on TiO2-NPs induced DNA damage (Vamanu et al., 2008; Gopalan et al., 2009; Barillet et al., 2010).

Furthermore, the flow-cytometric analysis of 24 h treated WISH cells has suggested the activation of DNA repair process with discernible cell cycle arrest in G2/M phase in damaged cells at higher TiO2-NPs concentrations. It is known that the cellular DNA repair mechanisms are highly conserved (Ferreira et al., 2002), and extensive DNA damage may lead to cell-cycle arrest and cell death (Konopa, 1988; Tsao et al., 1992). Most likely, the DNA damage induced with TiO2-NPs at lower concentrations up to 10 μg/ml could be adequately repaired during the G2/M phase, as no DNA damage (comet) was also observed at this concentration. However, the greater DNA damage occurred at a threshold concentration of 20 μg/ml TiO2-NPs, as evident with the appearance of a prominent comet tail due to irreparable double strand breaks. We have observed that the WISH cells were sensitive to alkaline conditions, which resulted in severe DNA damage even in untreated control cells. Therefore, the neutral comet assay was performed to determine the extent of induced DNA damage in this cell type at a threshold concentration of 20 μg/ml TiO2-NPs. However, in other cell lines such as goldfish skin (GFSk-S1) and rat kidney proximal (NRK-52E) cells, the DNA damage responses have been observed at much higher concentrations up to 100 μg/ml (Reeves et al., 2008; Barillet et al., 2010). It has been reported that the TiO2-NPs could directly bind to DNA or repair enzymes leading to the generation of strand breaks (Hartwig, 1998; Reeves et al., 2008). Most likely, the TiO2-NPs induced ˙OH radicals are responsible for the DNA damage in the exposed cells (Reeves et al., 2008). There are contradicting results in literature on exposure with different NPs at different stages of embryo development and also with the differences in experimental models (Challier et al., 1973; Bosman et al., 2005). Thus, the extent of induced genetic damage, and risk assessment of the nanomaterials and nanoproducts should be assessed prior to their larger applications in spite of their apparent extraordinary advantages.

5. Conclusion

It is concluded that this study for the first time explicitly demonstrated the cyto- and genotoxicity of TiO2-NPs in human amnion epithelial (WISH) cell line. Significant reduction in marker antioxidant levels and intracellular ROS generation suggested their role in inducing oxidative stress leading to DNA damage in treated cells. It is contemplated that the differential susceptibility of cell types could be due to differences in their metabolic rate, antioxidant enzyme machinery, and DNA repair capabilities, which may exhibit variability in TiO2-NPs induced toxic effects on human health. Furthermore, the TiO2-NPs predominantly present in aggregated form in culture medium, enter into cells mainly through endocytosis. Therefore, the extrapolation of *in vitro* dose response data to *in vivo* situation, i.e., in placenta or embryo is still a challenge. Further studies are warranted to investigate the particokinetics and rate of transport of TiO2-NPs in amniotic cells to ascertain more realistic NPs induced toxicity and risk assessment.

6. Conflict of interest

There is no conflict of interest.

Acknowledgements

Appendix A. Supplementary data

Supplementary data associated with this article can be found, in the online version, at doi:10.1016/j.tiv.2011.12.011.

References

Arys, A., Philippart, C., Dourov, N., He, Y., Le, Q.T., Pireaux, J.J., 1998. Analysis of titanium dental implants after failure of osseointegration: combined histological, electron microscopy, and X-ray photoelectron spectroscopy approach. J. Biomed. Mater. Res. 43, 300–312.

Baggs, R.B., Fern, J., Oberdorster, G., 1997. Regression of pulmonary lesions produced by inhaled titanium dioxide in rats. Vet. Pathol. 34, 592–597.

Barillet, S., Simon-Deckers, A., Herlin-Boime, N., Mayne-L'Hermite, M., Reynaud, C., Cassio, D., Gouget, B., Carrière, M., 2010. Toxicological consequences of TiO2, SiC nanoparticles and multi-walled carbon nanotubes exposure in several mammalian cell types: an *in vitro* study. J. Nanopart. Res. 12, 61–73.

Belyanskaya, L., Manser, P., Spohn, P., Bruinink, A., Wick, P., 2007. The reliability and limits of the MTT reduction assay for carbon nanotubes-cell interaction. Carbon 45, 2643–2648.

Bermudez, E., Mangum, J.B., Wong, B.A., Asgharian, B., Hext, P.M., Warheit, D.B., Everitt, J.I., 2004. Pulmonary responses of mice, rats, and hamsters to subchronic inhalation of ultrafine titanium dioxide particles. Toxicol. Sci. 77, 347–357.

Berne, B.J., Pecora, R., 2000. Dynamic Light Scattering: With Applications to Chemistry, Biology and Physics. Dover Publications.

Biondi, C., Fiorini, S., Boarini, I., Barbin, L., Cervellati, F., Ferrettia, M.E., Vesce, F., 2002. Effect of nitric oxide on arachidonic acid release from human amnion-like WISH cells. Placenta 23, 575–583.

Borm, P.J., Robbins, D., Haubold, S., Kuhlbusch, T., Fissan, H., Donaldson, K., Schins, R., Stone, V., Kreyling, W., Lademann, J., Krutmann, J., Warheit, D., Oberdorster, E., 2006. The potential risks of nanomaterials: a review carried out for ECETOC. Part. Fibre. Toxicol. 3, 11.

Bosman, S.J., Nieto, S.P., Patton, W.C., Jacobson, J.D., Corselli, J.U., Chan, P.J., 2005. Development of mammalian embryos exposed to mixed-size nanoparticles. Clin. Exp. Obstet. Gynecol. 32, 222–224.

Brien, W.W., Salvati, E.A., Betts, F., Bullough, P., Wright, T., Rimnac, C., Buly, R., Garvin, K., 1992. Metal levels in cemented total hip arthroplasty. A comparison of well-fixed and loose implants. Clin. Orthop. Relat. Res. 276, 66–74.

Buly, R.L., Huo, M.H., Salvati, E., Brien, W., Bansal, M., 1992. Titanium wear debris in failed cemented total hip arthroplasty. An analysis of 71 cases. J. Arthroplasty 7, 315–323.

Challier, J.C., Panigel, M., Meyer, E., 1973. Uptake of colloidal 198Au by fetal liver in rat, after direct intrafetal administration. Int. J. Nucl. Med. Biol. 1, 103–106.

Cunningham, B.W., Orbegoso, C.M., Dmitriev, A.E., Hallab, N.J., Sefter, J.C., McAfee, P.C., 2002. The effect of titanium particulate on development and maintenance of a posterolateral spinal arthrodesis: an *in vivo* rabbit model. Spine 27, 1971–1981.

Dalton, S., Janes, P.A., Jones, N.G., Nicholson, J.A., Hallam, K.R., Allen, G.C., 2002. Photocatalytic oxidation of NOx gases using TiO2: a surface spectroscopic approach. Environ. Pollut. 120, 415–422.

Darzynkiewicz, Z., Bruno, S., Del Bino, G., Gorczyca, W., Hotz, M.A., Lassota, P., Traganos, F., 1992. Features of apoptosis cells measured by flow cytometry. Cytometry 13, 795–808.

Donaldson, K., Stone, V., 2003. Current hypotheses on the mechanisms of toxicity of ultrafine particles. Annals. Ist. Super. Sanità. 39, 405–410.

Douglas, K.E., Dirk, V., Timothy, M.S., Bruce, J.S., 2000. Titanium nanoparticles move to the marketplace. Chem. Innov. 30, 30–35.

Driscoll, K.E., Maurer, J.K., 1991. Cytokine and growth factor release by alveolar macrophages: potential biomarkers of pulmonary toxicity. Toxicol. Pathol. 19, 398–405.

Ferreira, C.G., Epping, M., Kruyt, F.A., Giaccone, G., 2002. Apoptosis: target of cancer therapy. Clinic. Cancer Res. 8, 2024–2034.

Gao, Y., Masuda, Y., Seo, W., Ohta, H., Koumoto, K., 2004. TiO2 nanoparticles prepared using an aqueous peroxotitanate solution. Ceramics Int. 30, 1365–1368.

Gopalan, R.C., Osman, I.F., Amani, A., Matas, M.D., Anderson, D., 2009. The effect of zinc oxide and titanium dioxide nanoparticles in the Comet assay with UVA photoactivation of human sperm and lymphocytes. Nanotoxicology 3, 33–39.

Gurr, J.R., Wang, A.S., Chen, C.H., Jan, K.Y., 2005. Ultrafine titanium dioxide particles in the absence of photoactivation can induce oxidative damage to human bronchial epithelial cells. Toxicology 213, 66–73.

Hartwig, A., 1998. Carcinogenicity of metal compounds: possible role of DNA repair inhibition. Toxicol. Lett. 102–103, 239–355.

Hussain, S., Boland, S., Baeza-Squiban, A., Hamel, R., Thomassen, L.C., Martens, J.A., Billon-Galland, M.A., Fleury-Feith, J., Moisan, F., Pairon, J.C., Marano, F., 2009. Oxidative stress and proinflammatory effects of carbon black and titanium dioxide nanoparticles: role of particle surface area and internalized amount. Toxicology 260, 142–149.

Hussain, S., Thomassen, L.C.J., Ferecatu, I., Borot, M.C., Andreau, K., Martens, J.A., Fleury, J., Baeza-Squiban, A., Marano, F., Boland, S., 2010. Carbon black and titanium dioxide nanoparticles elicit distinct apoptotic pathways in bronchial epithelial cells. Part. Fiber. Toxicol. 7, 10.

Jin, C.Y., Zhu, B.S., Wang, X.F., Lu, Q.H., 2008. Cytotoxicity of titanium dioxide nanoparticles in mouse fibroblast cells. Chem. Res. Toxicol. 21, 1871–1877.

Keelan, J.A., Helliwell, R.J.A., Nijmeijer, B.E., Berry, E.B.E., Sato, T.A., Marvin, K.W., Mitchell, M.D., Gilmour, R.S., 2001. 15-deoxy-Δ12, 14-prostaglandin J2-induced apoptosis in amnion-like WISH cells. Prostag. Oth. Lipid M 66, 265–282.

Konopa, J., 1988. G_2 block induced by DNA crosslinking agents and its possible consequence. Biochem. Pharmacol. 37, 2303–2309.

Kumar, D., Lundgrena, D.W., Moore, R.M., Silver, R.J., Moore, J.J., 2004. Hydrogen Peroxide Induced Apoptosis in Amnion-derived WISH Cells is not Inhibited by Vitamin C. Placenta 25, 266–272.

Lacasana, M., Esplugues, A., Ballester, F., 2005. Exposure to ambient air pollution and prenatal and early childhood health effects. Eur. J. Epidemiol. 20, 183–199.

Limbach, L.K., Li, Y.C., Grass, R.N., Brunner, T.J., Hintermann, M.A., Muller, M., Gunther, D., Stark, W.J., 2005. Oxide nanoparticle uptake in human lung fibroblasts: effects of particle size, agglomeration, and diffusion at low concentrations. Environ. Sci. Tech. 39, 9370–9376.

Lison, D., Thomassen, L.C., Rabolli, V., Gonzalez, L., Napierska, D., Seo, J.W., Kirsch-Volders, M., Hoet, P., Kirschhock, C.E., Martens, J.A., 2008. Nominal and effective dosimetry of silica nanoparticles in cytotoxicity assays. Toxicol. Sci. 104, 155–162.

Long, T.C., Tajuba, J., Sama, P., Saleh, N., Swartz, C., Parker, J., Hester, S., Lowry, G.V., Veronesi, B., 2007. Nanosize titanium dioxide stimulates reactive oxygen species in brain microglia and damages neurons in vitro. Environ. Health. Perspect. 115, 1631–1637.

Lundgren, D.W., Moore, R.M., Collins, P.L., Moore, J.J., 1997. Hypotonic stress increases cyclooxygenase-2 expression and prostaglandin release from amnion-derived WISH cells. J. Biol. Chem. 272, 20118–20124.

Lynch, I., Dawson, K.A., Linse, S., 2006. Detecting cryptic epitopes created by nanoparticles. Sci. STKE 327, 14.

Messer, J., Reynolds, M., Stoddard, L., Zhitkovich, A., 2006. Causes of DNA single-strand breaks during reduction of chromate by glutathione in vitro and in cells. Free. Rad. Biol. Med. 40, 1981–1992.

Moore, R.M., Lundgren, D.W., Silver, R.J., Moore, J.J., 2002. Lactosylceramide induced apoptosis in primary amnion cells and amnion-derived WISH cells. J. Soc. Gynecol. Investig. 9, 282–289.

Nel, A., Xia, T., Madler, L., Li, N., 2006. Toxic potential of materials at the nanolevel. Science 311, 622–627.

Nemmar, A., Melghit, K., Al-Salam, S., Zia, S., Dhanasekaran, S., Attoub, S., Al-Amri, I., Ali, B.H., 2011. Acute respiratory and systemic toxicity of pulmonary exposure to rutile Fe-doped TiO(2) nanorods. Toxicology 279, 167–175.

Oberdörster, G., 2000. Pulmonary effects of inhaled ultra-fine particles. Int. Arch. Occup. Environ. Health 74, 1–8.

Oberdörster, G., Ferin, J., Lehnert, B.E., 1994. Correlation between particle size, in vivo particle persistence, and lung injury. Environ. Health Perspect. 102, 173–179.

Oberdörster, G., Oberdorster, E., Oberdorster, J., 2005. Nanotoxicology: an emerging discipline evolving from studies of ultrafine particles. Environ. Health. Perspect. 113, 823–839.

Omidkhoda, A., Mozdarani, H., Movasaghpoor, A., Fatholah, A.K.P., 2007. Study of apoptosis in labeled mesenchymal stem cells with superparamagnetic iron oxide using neutral comet assay. Toxicol. In Vitro 21, 1191–1196.

Park, S., Lee, Y.K., Jung, M., Kim, K.H., Chung, N., Ahn, E.K., Lim, Y., Lee, K.H., 2007. Cellular toxicity of various inhalable metal nanoparticles on human alveolar epithelial cells. Inhal. Toxicol. 19, 59–65.

Reeves, J.F., Davies, S.J., Dodd, N.J.F., Jha, A.N., 2008. Hydroxyl radicals (˙OH) are associated with titanium dioxide (TiO$_2$) nanoparticle-induced cytotoxicity and oxidative DNA damage in fish cells. Mutat. Res. 640, 113–122.

Saquib, Q., Al-Khedhairy, A.A., Al-Arifi, S., Dhawan, A., Musarrat, J., 2009. Assessment of methyl thiophanate-Cu (II) induced DNA damage in human lymphocytes. Toxicol. In Vitro 23, 848–854.

Semmler-Behnke, M., Fertsch, S., Schmid, G., Wenk, A., Kreyling, W.G., 2007. Uptake of 1.4 nm versus 18 nm gold nanoparticles in secondary target organs is size dependent in control and pregnant rats after intratrecheal or intravenous application. In: EuroNanoForum 2007-Nanotechnology in Industrial Applications. Luxembourg: European Communities, pp. 102–104.

Shukla, R.K., Sharma, V., Pandey, A.K., Singh, S., Sultana, S., Dhawan, A., 2011. ROS-mediated genotoxicity induced by titanium dioxide nanoparticles in human epidermal cells. Toxicol. In Vitro 25, 231–241.

Siddiqui, M.A., Singh, G., Kashyap, M.P., Khanna, V.K., Yadav, S., Chandra, D., Pant, A.B., 2008. Influence of cytotoxic doses of 4-hydroxynonenal on selected neurotransmitter receptors in PC-12 cells. Toxicol. In Vitro 22, 1681–1688.

Siddiqui, M.A., Kashyap, M.P., Kumar, V., Al-Khedhairy, A.A., Musarrat, J., Pant, A.B., 2010. Protective potential of trans-resveratrol against 4-hydroxynonenal induced damage in PC12 cells. Toxicol. In Vitro 24, 1592–1598.

Singh, S., Shi, T., Duffin, R., Albrecht, C., Berlo, D.V., Höhr, D., Fubini, B., Martra, G., Fenoglio, I., Borm, P.J.A., Schins, R.P.F., 2007. Endocytosis, oxidative stress and IL-8 expression in human lung epithelial cells upon treatment with fine and ultrafine TiO2: Role of the specific surface area and of surface methylation of the particles. Toxicol. Appl. Pharmacol. 222, 141–151.

Stone, V., Shaw, J., Brown, D.M., MacNee, W., Faux, S.P., Donaldson, K., 1998. The role of oxidative stress in the prolonged inhibitory effect of ultrafine carbon black on epithelial cell function. Toxicol. In Vitro 12, 649–659.

Takeda, K., Suzuki, K.I., Ishihara, A., Kubo-Irie, M., Fujimoto, R., Tabata, M., Oshio, S., Nihei, Y., Ihara, T., Sugamata, M., 2009. Nanoparticles transferred from pregnant mice to their offspring can damage the genital and cranial nerve systems. J. Health Sci. 55, 95–102.

Tauc, J., Grigorovici, R., Vancu, A., 2006. Optical properties and electronic structure of amorphous germanium. Physica Status Solidi (b) 15, 627–637.

Teeguarden, J.G., Hinderliter, P.M., Orr, G., Thrall, B.D., Pounds, J.G., 2007. Particokinetics in vitro: dosimetry considerations for in vitro nanoparticle toxicity assessments. Toxicol. Sci. 95, 300–312.

Thomas, C.L., Navid, S., Robert, D.T., 2006. Titanium dioxide (P25) produces reactive oxygen species in immortalized brain microglia (BV2): implications for nanoparticle neurotoxicity. Environ. Sci. Technol. 40, 4346–4352.

Tian, F., Razansky, D., Estrada, G.G., Semmler-Behnke, M., Beyerle, A., Kreyling, W., Ntziachristos, V., Stoeger, T., 2009. Surface modification and size dependence in particle translocation during early embryonic development. Inhal. Toxicol. 21, 92–96.

Tsao, Y.P., D'Arpa, P., Liu, L.F., 1992. The involvement of active DNA synthesis in camptothecin-induced G_2 arrest: altered regulation of p34cdc2/cyclin B. Cancer Res. 52, 1823–1829.

Vamanu, C.I., Cimpan, M.R., Høl, P.J., Sørnes, S., Lie, S.A., Gjerdet, N.R., 2008. Induction of cell death by TiO$_2$ NPs: Studies on a human monoblastoid cell line. Toxicol. In Vitro 22, 1689–1696.

Vevers, W.F., Jha, A.N., 2008. Genotoxic and cytotoxic potential of titanium dioxide (TiO$_2$) nanoparticles on fish cells in vitro. Ecotoxicology 17, 410–420.

Wang, J., Zhou, G., Chen, C., Yu, H., Wang, T., Ma, Y., Jia, G., Gao, Y., Li, B., Sun, J., Li, Y., Jiao, F., Zhao, Y., Chai, Z., 2007. Acute toxicity and biodistribution of different sized titanium dioxide particles in mice after oral administration. Toxicol. Lett. 168, 176–185.

Warheit, D.B., Webb, T.R., Reed, K.L., Frerichs, S., Sayes, C.M., 2007. Pulmonary toxicity study in rats with three forms of ultrafine-TiO2 particles: differential responses related to surface properties. Toxicology 230, 90–104.

Wick, P., Malek, A., Manser, P., Meili, D., Maeder-Althaus, X., Diener, L., Diener, P.A., Zisch, A., Krug, H.F., Mandach, U.V., 2010. Barrier capacity of human placenta for nanosized materials. Environ. Health Perspect. 118, 432–436.

Wu, C.W., Ping, Y.H., Yen, J.C., Chang, C.Y., Wang, S.F., Yeh, C.L., Chi, C.W., Lee, H.C., 2007. Enhanced oxidative stress and aberrant mitochondrial biogenesis in human neuroblastoma SH-SY5Y cells during methamphetamine induced apoptosis. Toxicol. Appl. Pharmacol. 220, 243–251.

Xia, T., Kovochich, M., Brant, J., Hotze, M., Semp, J., Oberley, T., Sioutas, C., Yeh, J.I., Wiesner, M.R., Nel, A.E., 2006. Comparison of the abilities of ambient and manufactured nanoparticles to induce cellular toxicity according to an oxidative stress paradigm. Nano Lett. 6, 1794–1807.

Yoko, T., Kamiya, K., Tanaka, K., 1990. Preparation of multiple oxide barium titanate (BaTiO$_3$) fibers by the sol–gel method. J. Mater. Sci. 25, 3922–3929.

Zhang, R., Gao, L., 2002. Synthesis of nanosized TiO$_2$ by hydrolysis of alkoxide titanium in micelles. Key. Eng. Mater. 573, 224–226.

Zhang, J., Boyd, I., Sullivan, B.J.O., Hurley, P.K., Kelly, P.V., Senateur, J.P., 2002. Nanocrystalline TiO$_2$ thin films studied by optical, XRD and FTIR spectroscope. J. Non-Cryst. Solid 303, 134–138.

Zhao, J., Bowman, L., Zhang, X., Vallyathan, V., Young, S.H., Castranova, V., Ding, M., 2009. Titanium dioxide (TiO$_2$) nanoparticles induce JB6 cell apoptosis through activation of the caspase-8/bid and mitochondrial pathways. J. Toxicol. Environ. Health 72, 1141–11511.